Journal of Ceramic Processing Research. Vol. 18, No. 5, pp. 399~403 (2017)

JOURNAL OF
Ceramic
Processing Research

Microstructure of titanium aluminide prepared by centrifugal investment casting for automotive turbocharger

Jong Bum Park[a,b], Jung-Il Lee[b] and Jeong Ho Ryu[b]*
[a]*Chunji Corporation, Yeoju, Gyeonggi 12663, Korea*
[b]*Department of Materials Science and Engineering, Korea National University of Transportation, Chungju, Chungbuk 27469, Korea*

From a technical perspective, many of the unique properties of titanium aluminides that make them attractive for high-temperature structural applications also make the processing of these alloys into useful products challenging. Cast titanium aluminide (TiAl) is on the verge of commercialization, particularly in the vehicle industry, owing to its low production cost. In this study, the centrifugal castability of a TiAl (Ti-47%Al, mole fraction) turbocharger was investigated by simulation. Actual casting was carried out in vacuum using an induction melting furnace coupled to an Al_2O_3 crucible. Experimental verification indicated that the numerical simulation results were in agreement with the experimental results. The crystal structure, microstructure, and chemical composition of the TiAl prepared by centrifugal casting were studied by X-ray diffractometry, optical microscopy, field emission scanning electron microscopy (FE-SEM) and energy dispersive spectroscopy (EDS). The FE-SEM and EDS examinations of the TiAl casting showed that the thickness of the oxide layer (α-case) was typically less than 30 μm.

Key words: Titanium aluminide (TiAl), Centrifugal casting, Numerical simulation, Turbocharger, α-case.

Introduction

Owing to their high specific strength, excellent high-temperature properties and good oxidation resistance [1-3], intermetallic titanium aluminide (TiAl) alloys are potential high-temperature structural materials for aerospace and automobile applications such as low-pressure turbine blades, turbochargers and exhaust valves [4-6]. Owing chiefly to these properties, titanium aluminides provide significant potential as alternatives for innovative applications in advanced energy conversion systems, as they may be used to replace heavier nickel-based superalloys at moderately high temperatures of ~ 700 °C. The most important pay-off areas in the automotive and aero industries have been assessed in recent studies [7-9]. The most important requirement for such applications is a good balance of mechanical properties over a wide temperature range. This includes damage tolerance, ductility, fracture toughness, fatigue strength, and creep resistance.

Casting TiAl alloys have drawbacks like large solidification shrinkage, high chemical reactivity, and poor ductility, which result in misruns, porosity, and crack defects in cast products [10]. To obtain perfect quality castings, it is essential to select the appropriate casting process and technological parameters. Considering the efficiency and cost, the traditional trial and error method is no longer suitable for the need of modern industrial development because of the high cost and long experimental period. The numerical simulation trial and error method forecasts defects such as shrinkages and cracks. The conventional trial and error method for designing a casting process based on experience or manual craft often results in higher costs and longer cycles of preproduction. One typical case is centrifugal casting. The centrifugal casting of investment molds to produce turbochargers is restricted in use, because the quality of products is highly sensitive to damage due to inappropriate processing conditions and mold design. Therefore, a design based on computer simulation and real-time radiography technology is needed because it can improve quality, reduce cost and shorten preproduction time [11-13].

In this work, the numerical simulation method was used to study the investment casting process of a TiAl alloy for turbochargers by the centrifugal process. Actual casting experiments were carried out to validate the simulation results and to analyze the crystal structure and microstructure.

Experimental

Mathematical model establishments and parameters setting of casting simulation

The liquid is assumed to be an incompressible Newtonian fluid and the governing equations in the filling and solidification states are given by the Navier-

*Corresponding author:
Tel : +82-43-841-5384
Fax: +82-43-841-5380
E-mail: jhryu@ut.ac.kr

Stokes equation [14]:

$$\rho\left(\frac{\partial u}{\partial t}+u\frac{\partial u}{\partial x}+v\frac{\partial u}{\partial y}+w\frac{\partial u}{\partial z}\right)=-\frac{\partial p}{\partial x}=\rho g_x+\mu\left(\frac{\partial^2 u}{\partial x^2}+\frac{\partial^2 u}{\partial y^2}+\frac{\partial^2 u}{\partial z^2}\right) \quad (1)$$

$$\rho\left(\frac{\partial v}{\partial t}+u\frac{\partial v}{\partial x}+v\frac{\partial v}{\partial y}+w\frac{\partial v}{\partial z}\right)=-\frac{\partial p}{\partial y}=\rho g_y+\mu\left(\frac{\partial^2 v}{\partial x^2}+\frac{\partial^2 v}{\partial y^2}+\frac{\partial^2 v}{\partial z^2}\right) \quad (2)$$

$$\rho\left(\frac{\partial w}{\partial t}+u\frac{\partial w}{\partial x}+v\frac{\partial w}{\partial y}+w\frac{\partial w}{\partial z}\right)=-\frac{\partial p}{\partial y}=\rho g_y+\mu\left(\frac{\partial^2 w}{\partial x^2}+\frac{\partial^2 w}{\partial y^2}+\frac{\partial^2 w}{\partial z^2}\right) \quad (3)$$

Continuity equation:

$$\frac{\partial u}{\partial x}+\frac{\partial v}{\partial y}+\frac{\partial w}{\partial z}=0 \quad (4)$$

Heat transfer equation:

$$\rho C_p\left(\frac{\partial w}{\partial t}+u\frac{\partial T}{\partial x}+v\frac{\partial T}{\partial y}+w\frac{\partial T}{\partial z}\right)=\lambda\left(\frac{\partial^2 T}{\partial x^2}+\frac{\partial^2 T}{\partial y^2}+\frac{\partial^2 T}{\partial z^2}\right)+L\frac{\partial f_s}{\partial t} \quad (5)$$

Here, ρ is the density; u, v, and w are the velocity vectors; t is the time; μ is the dynamic viscosity of the liquid metal; g_x, g_y and g_z are the gravitational acceleration vectors in the x, y and z directions, respectively; P is the pressure; C_p is the specific heat of the molten metal; λ is the thermal conductivity; L is the latent heat; f_s is the solid phase ratio at the solidification stage.

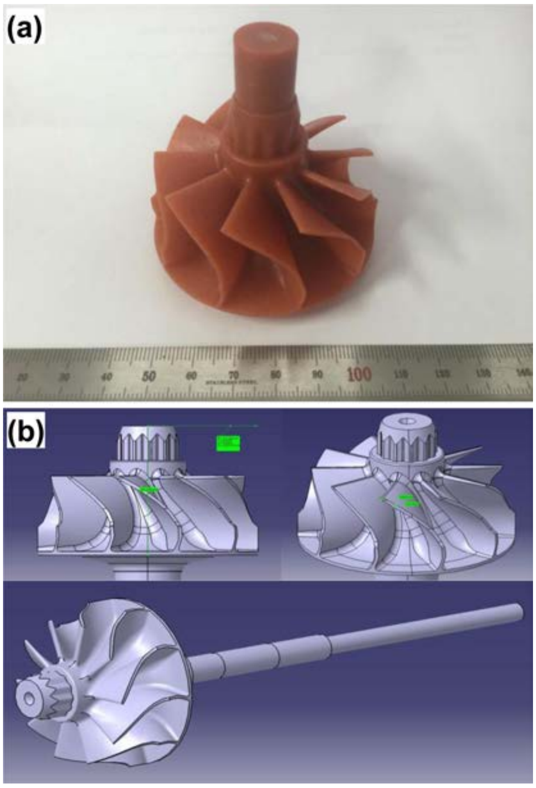

Fig. 1. Wax pattern (a) and virtual three-dimensional model (b) of single turbocharger designed using Pro/E software.

Table 1. Thermodynamic parameters of titanium aluminide and mold material.

TiAl	Value	Ceramic mold	Value
Conductivity [$W \cdot m^{-1} \cdot K^{-1}$]	15-26	Conductivity [$W \cdot m^{-1} \cdot K^{-1}$]	0.83-0.97
Density [$kg \cdot m^{-3}$]	4135-4513	Density [$kg \cdot m^{-3}$]	2780
Specific heat [$kJ \cdot kg^{-1} \cdot K^{-1}$]	0.63-1.02	Specific heat [$kJ \cdot kg^{-1} \cdot K^{-1}$]	0.44-0.85
Enthalpy [$kJ \cdot kg^{-1}$]	330		
Liquidus [°C]	1578		
Solidus [°C]	1405		
Viscosity [Pa·s]	$(4.65\text{-}8.80) \times 10^{-3}$		

The actual wax part of the turbocharger is shown in Fig. 1(a). A virtual three-dimensional model of a single turbocharger was designed using Pro/E software, seen in Fig. 1(b). A finite element software (Procast) was used to simulate the filling and solidification processes of investment casting. The thermodynamic parameters of TiAl and the mold material, which were calculated using the Pandat software, are listed in Table 1. Gravity-casting process parameters were optimized using an orthogonal experiment, i.e., a casting temperature of 1650 °C, pouring speed of 0.5 ms^{-1}, mold preheating temperature of 500 °C, and heat transfer coefficient of 500 $W \cdot m^{-2} \cdot K^{-1}$. The central rotational speed was calculated by using the following formula according to the g-Force criteria [15]:

$$n=29.9\sqrt{\frac{G}{r}} \quad (6)$$

where n is the centrifugal rotational speed (r/min), r is the radius of the inner surface of the casting mold (mm), and G is the gravity coefficient whose value is 40-110. According to Eq. (6), the centrifugal rotational speed was calculated to be 200-400 $r \cdot min^{-1}$. The actual value used in simulation and experiment was the median value of 300 $r \cdot min^{-1}$.

Centrifugal investment casting and characterization

The nominal composition of the actual casting material was Ti-47Al-2.5Nb-1.5Cr (atomic %). The ceramic mold, which comprised mainly Al_2O_3, had a thickness of 8-10 mm. Al_2O_3 was selected for the mold material as it combines handling strength, formability, permeability, and collapsibility to ensure dimensional accuracy of castings and cost competitiveness [16]. The actual pouring experiment was carried out using a vacuum induction suspended furnace in an Ar atmosphere. The centrifugal investment casting furnace

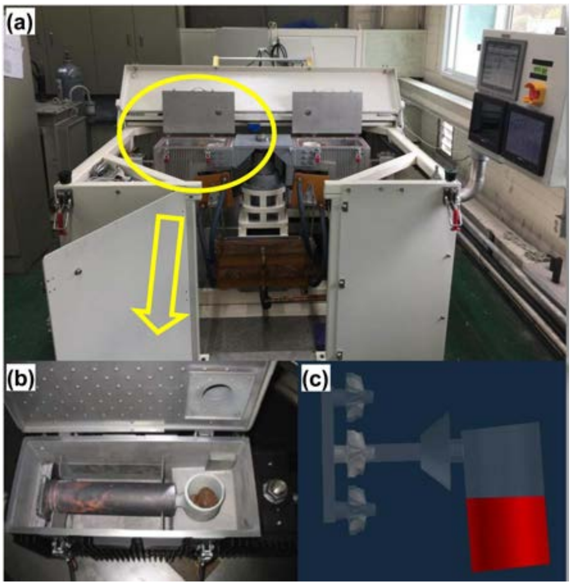

Fig. 2. Photograph of the centrifugal furnace installation (a,b) and the complete geometry (c) of the turbocharger investment for simulation.

is shown in Fig. 2(a,b). Before centrifugal casting, the preheated mold was fixed on the centrifugal rotary wheel at the top of the furnace chamber. The one-step melting and centrifugal casting process was adopted to reduce the cost of castings as shown in Fig. 2(c). This means that when the temperature of the molten alloy and rotation speed of the ceramic mold are adjusted to pre-determined parameters, the liquid is directly poured into the turning ceramic mold.

The crystal structure was analyzed by X-ray diffractometry (XRD, Philips X-pert system with Cu-Kα radiation). Microstructural examination was performed using optical microscopy (OM) and field emission scanning electron microscopy (FE-SEM, Hitachi S-4700) equipped with energy dispersive spectroscopy (EDS). For OM and FE-SEM examination, polished surfaces of the centrifugal-cast bulk solid samples were etched with Kroll's solution (5% HNO_3 + 3% HF + 92% H_2O, volume fraction).

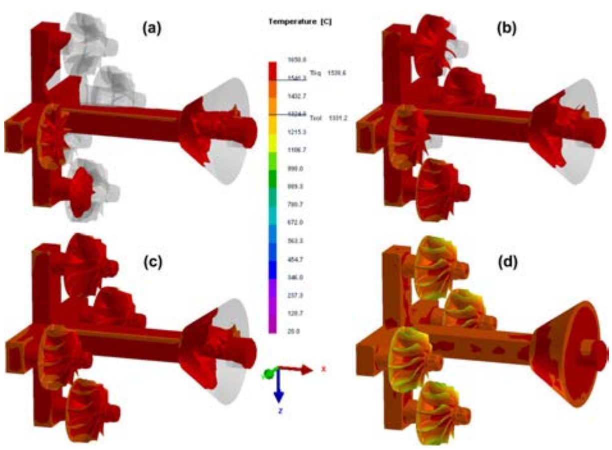

Fig. 3. Centrifugal processing simulation after the melt is directly poured into the turning ceramic mold. Temperature distribution after (a) 0.6, (b) 0.76, (c) 0.77 and (d) 1.1 sec.

Fig. 4. Photograph of titanium aluminide turbocharger prepared by centrifugal investment casting.

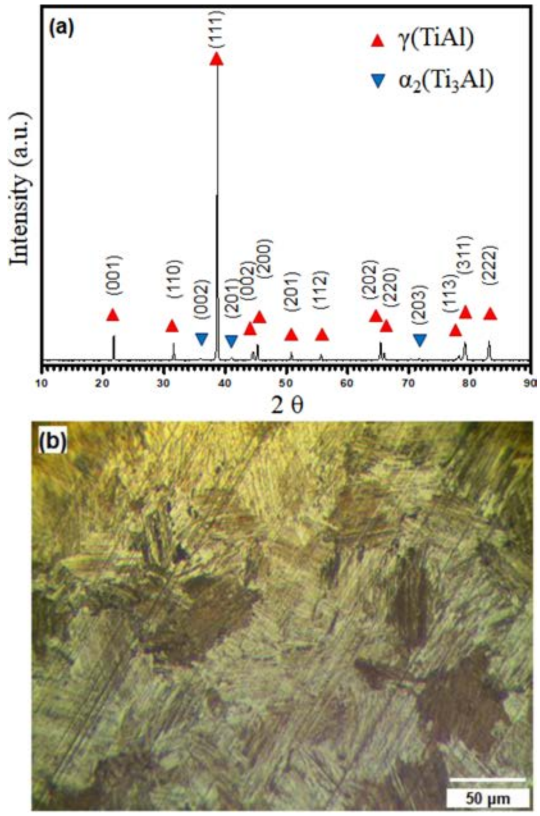

Fig. 5. XRD pattern (a) and optical microstructure (b) of the titanium aluminide sample prepared by centrifugal investment casting.

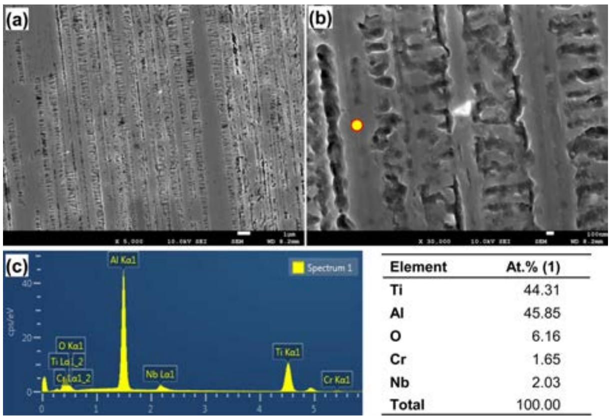

Element	At.% (1)
Ti	44.31
Al	45.85
O	6.16
Cr	1.65
Nb	2.03
Total	100.00

Fig. 6. FE-SEM microstructure (a,b) and chemical composition (c) of the aluminide sample prepared by centrifugal investment casting.

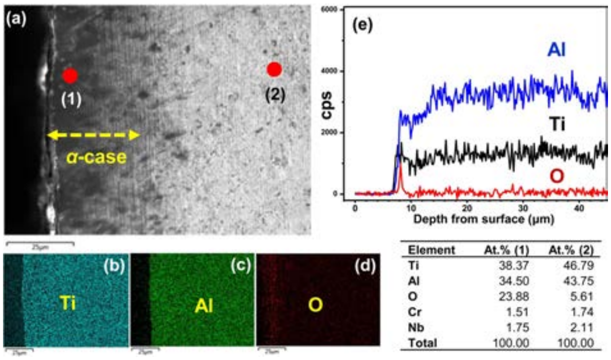

Element	At.% (1)	At.% (2)
Ti	38.37	46.79
Al	34.50	43.75
O	23.88	5.61
Cr	1.51	1.74
Nb	1.75	2.11
Total	100.00	100.00

Fig. 7. Cross-sectional FE-SEM microstructure (a), EDX elemental maps (b-d), and line profile (e) of the titanium aluminide sample prepared by centrifugal casting.

Results and Discussion

Fig. 3 shows the centrifugal casting simulation processes and turbochargers. In the gravity-casting simulations [15], the molten metal flowed along the suction side of the turbocharger. After reaching the blade, the molten metal flowed back into the pressure side of the blade. The metal fluid fully filled the mold cavity 1 s after pouring. Owing to the effects of centrifugal force, the molten metal flowed along the pressure side at first, shown in Fig. 3. The cavity was fully filled 0.77 s after pouring, 0.23 s faster than in gravity casting. Fig. 4 shows a real cast turbine wheel prepared by the centrifugal casting process. Misrun defects were not observed in the trailing edge of the sample. The trailing edge, which is the thinnest edge of the turbine wheel, was the last portion filled by molten metal in the gravity-casting process, resulting in the generation of misrun defects [11, 15]. On the other hand, molten metal fills the thinnest edge in the centrifugal casting process because of centrifugal force, which is beneficial for obtaining a complete turbine wheel.

Fig. 5(a) shows the XRD result of the TiAl sample prepared using centrifugal casting. The XRD analysis proved the existence of a γ-ordered TiAl phase with tetragonal lattices ($a = 0.4016$ nm and $c = 0.4073$ nm) and a c/a ratio of 1.014 as the major phase and an α_2-ordered Ti_3Al phase with a close-packed-hexagonal lattice ($a = 0.5753$ nm and $c = 0.4644$ nm) as the minor phase. The c/a ratio of the major γ-TiAl phase is close to 1.02, which corresponds to the equiatomic TiAl composition, whereas tetragonality increases up to $c/a = 1.03$ with increasing aluminum concentration [17]. No peak of the retained ordered β(B2) phase, which crystallizes in the CsCl structure, was detected. Unlike castings of a commercial alloy (Ti64, Ti-6Al-4V) wherein a peak of TiC and/or TiCN was detected owing to the reaction of the melt and carbon crucible [18], no carbon was detected in the prepared casing in this case. Optical microscope clearly reveals that coarse grains possessed a fully lamellar microstructure where the lamellae were mostly γ-TiAl grains intermixed with dark lamellae of the α_2 phase as shown in Fig. 5(b).

Fig. 6(a,b) shows the FE-SEM microstructure of the TiAl sample prepared by centrifugal casting at different magnifications. As shown in Fig. 6(a,b), this microstructure mainly consisted of lamellar colonies of γ-TiAl grains. Fig. 6(c,d) represents the EDS spectrum and chemical composition table for the yellow region in Fig. 6(b). The chemical composition measured by EDS corresponds to the raw casting composition. Oxygen contamination was detected over 6.0 at% despite the short melting time, which is due to the unavoidable contact between the TiAl melt and the Al_2O_3 ceramic mold [19]. Contact between the TiAl melt and these ceramics is likely to introduce ceramic-induced impurities and inclusions in the melt and could therefore lead to a negative impact on the properties of the resulting TiAl cast material [20].

Pattnaik et al. [21] demonstrated that titanium investment casing is one of the most efficient manufacturing processes for obtaining near-net-shaped intricate components. However, the high melting points and reactivities of these alloys induce the decomposition of mold materials, resulting in interface mold-metal reactions during casting. As Chamorro et al. [22] pointed out, several process conditions affect mold-metal reaction mechanisms; the surrounding atmosphere, titanium pouring temperature, stability of the refractory mold material, and mold temperature are the most relevant ones. Yu et al. [23] further empirically demonstrated that Al_2O_3 decomposition occurs and the detrimental reacted skin, known as the α-case, remains on the surface of the final casting.

Fig. 7 shows the microstructure (a), EDX elemental mapping (b-d) and line profile (e) of the TiAl sample prepared by centrifugal casting. Fig. 7(a) shows the cross-sectional FE-SEM microstructure of the surface on the sample. The two marked points indicate the sites of EDS composition analysis presented in the Table accompanying Fig. 7. From the composition and line scan analyses, the fine structure of the oxidation zone (α-case) was determined and is indicated in Fig. 7(a). The oxygen owing to the α-case was detected to a depth of ~ 30 μm.

Summary

The centrifugal investment casting process was simulated using TiAl (Ti-47%Al, mole fraction) for casting a turbocharger wheel. The simulated and actual results are consistent. The microstructure and chemical composition were analyzed. The cavity was fully filled at 0.77 s after pouring, which was faster than with gravity casting. The turbocharger wheel prepared by centrifugal casting did not have misrun defects in the trailing edge. XRD analysis proved the existence of a γ-ordered TiAl phase with tetragonal lattices as the major phase and α_2-ordered Ti_3Al phase with close-packed-hexagonal lattices as the minor phase. The chemical composition measured by EDS corresponded to the raw casting composition. The FE-SEM and EDS examinations of the TiAl casting showed that the thickness of the oxide layer (α-case) was typically less than 30 μm.

Acknowledgements

This work was supported by the Technological Innovation R&D Program (S2296345) funded by the Small and Medium Business Administration (SMBA, Korea).

References

1. T. Noda, Intermetallics 6 (1998) 709-713.
2. Y.W. Kim, J. Met. 46 (1994) 30-39.
3. R.V. Ramanujan, Int. Mater. Rev. 45(6) (2000) 217-240.
4. K. Clemens, H. Kestler, Adv. Eng. Mater. 2(9) (2000) 551-570.
5. R.M. Imayev, V.M. Imayev, M. Oehring, F. Appel, Intermetallics 15 (2007) 451-460.
6. T. Tetsui, Mater. Sci. Eng. A 329-331 (2002) 582-588.
7. H. Clemens, S. Mayer, Adv. Eng. Mater. 15 (2013) 191-215.
8. J. Soyama, M. Oehring, W. Limberg, T. Ebel, K.U. Kainer, F. Pyczak, Mater. Des. 84 (2015) 87-94.
9. J.D.H. Paul, U. Lorenz, M. Oehring, F. Appel, Intermetallics 32 (2013) 318-328.
10. T.I. Nazarova, V.M. Imayev, R.M. Imayev, H.-J. Fecht, Intermetallics 82 (2017) 26-31.
11. P.X. Fu, X.H. Kang, Y.C. Ma, K. Liu, D.Z. Li, Y.Y. Li, Intermetallics 16 (2008) 130-138.
12. B.H. Hu, K.K. Tong, X.P. Niu, I. Pinwill, J. Mater. Process. Technol. 105 (2000) 128-133.
13. D.Z. Li, J. Campbell, Y.Y. Li, J. Mater. Process. Technol. 148 (2004) 310-316.
14. G.F. Mi, X.Y. Liu, K.F. Wang, H.Z. Fu, J. Iron Steel Res. Int. 16(4) (2009) 12-17.
15. L. Yang, L.H. Chai, Y.F. Liang, Y.W. Zhang, C.L. Bao, S.B. Liu, J.P. Lin, Intermetallics 66 (2015) 149-155.
16. S-Y. Sung, Y.-J. Kim, Intermetallics 15 (2007) 468-474.
17. J.Y. Jung, J.K. Park, C.H. Chun, Intermetallics 7 (1999) 1033-1041.
18. M.T. Jovanović, S. Tadić, S. Zec, Z. Mišković, I. Bobić, Mater. Des. 27 (2006) 192-199.
19. H.Z. Niu, Y.Y. Chen, S.L. Xiao, L.J. Xu, Intermetallics 31 (2012) 225-231.
20. T. Tetsui, T. Kobayashi, T. Ueno, H. Harada, Intermetallics 31 (2012) 274-281.
21. S. Pattnaik, D.B. Karunakar, P.K. Jha, J. Mater. Process. Technol. 212 (11) 2332-2348.
22. X. Chamorro, N. Herrero-Dorca, P.P. Podríguez, U. Andrés, Z. Azilgain, J. Mater. Process. Technol. 243 (2017) 75-81.